Available online at www.sciencedirect.com
SCIENCE DIRECT
Tectonophysics 412 (2006) 217–235
TECTONOPHYSICS
www.elsevier.com/locate/tecto

Seismic activity at the western Pyrenean edge

M. Ruiz [a,*], J. Gallart [a], J. Díaz [a], C. Olivera [b], D. Pedreira [c], C. López [c], J.M. González-Cortina [c], J.A. Pulgar [c]

[a] Dpt. Geofísica i Tectònica, Institut de Ciències de la Terra 'Jaume Almera' IJA-CSIC, Solé Sabaris s/n 08028 Barcelona, Spain
[b] Institut Cartogràfic de Catalunya, Parc de Montjuic s/n, 08038 Barcelona, Spain
[c] Dpt. Geología, Universidad de Oviedo, Arias de Velasco s/n, 33005 Oviedo, Spain

Received 27 August 2004; received in revised form 7 October 2005; accepted 16 October 2005
Available online 19 December 2005

Abstract

The present-day seismicity at the westernmost part of the Pyrenean domain reported from permanent networks is of low to moderate magnitude. However, it is poorly constrained due to the scarce station coverage of the area. We present new seismic data collected from a temporary network deployed there for 17 months that provides an enhanced image of the seismic activity and its tectonic implications. Our results delineate the westward continuity of the E–W Pyrenean band of seismicity, through the Variscan Basque Massifs along the Leiza Fault, ending up at the Hendaya Fault. This seismicity belt is distributed on a crustal scale, dipping northward to almost 30 km depth. Other relevant seismic events located in the area can be related to the central segment of the Pamplona fault, and to different E–W thrust structures.

Keywords: Western Pyrenees; Temporary array; Seismicity; Seismotectonics

1. Introduction

New seismic data have been collected in the northern part of the Iberian Peninsula (Fig. 1), from the Pyrenees to Galicia, using temporary networks deployed in the framework of the Spanish Research Project GASPI. The aim of that project was two-fold: i) the lithospheric structure in relation to Variscan and Alpine tectonics as investigated from passive seismic methods, using the teleseismic receiver function technique (Díaz et al., 2003) and testing the presence of anisotropy (Díaz et al., 2002), and ii) the present-day seismotectonic activity. To reach these objectives, up to three seismic networks, covering the western end of the Pyrenean range, the Cantabrian Mountains and the Galicia region have been deployed in different periods between 1999 and 2002.

This contribution focuses on the analysis of the seismic activity at the western termination of the Pyrenean range. The seismicity of this region is poorly constrained from a low-density coverage of permanent stations. The area is monitored by only two instruments of the Spanish IGN (National Geographic Institute) network, and the few westernmost instruments of the RENASS (Réseau National de Surveillance Sismique) and CEA (Atomic Energy Commission) French's Pyrenean networks, with a clearly inappropriate distribution to produce accurate seismicity maps (Fig. 2). The new data obtained from the temporary array, combined with data from permanent instruments, has improved the mapping of local and regional earthquake distribution in relation with different tectonic structures on a crustal scale.

* Corresponding author. Tel.: +34 93 409 54 10; fax: +34 93 411 00 12.
E-mail address: mruiz@ija.csic.es (M. Ruiz).

0040-1951/$ - see front matter © 2005 Elsevier B.V. All rights reserved.
doi:10.1016/j.tecto.2005.10.034

2. Geological setting

The study area includes the westernmost Pyrenean range and the beginning of its structural transition to the Cantabrian Mountains through the Basque–Cantabrian basin (Fig. 1). The region was affected by the Variscan (Matte, 1991) and Alpine orogenies (Choukroune, 1992; Muñoz, 1992), separated by a large Mesozoic extensional period which resulted in the opening of the Bay of Biscay and the formation of the Cantabrian Margin (Rat, 1988; Alonso et al., 1996; Pulgar et al., 1996).

The main Pyrenean structures in this area show a roughly E–W orientation, with the Paleozoic Axial Zone (PAZ) in its central part, bordered by the North Pyrenean Zone (NPZ) and the South Pyrenean Zone (SPZ), which are Mesozoic and Cenozoic units overthrusting the Tertiary Aquitaine and Ebro foreland basins. The Basque–Cantabrian basin to the west of the study area is a Mesozoic extensional basin which was inverted in Cenozoic times during the Pyrenean orogeny (Alonso et al., 1996; Pulgar et al., 1996; Pedreira et al., 2003). From Triassic to Albian times, an intense extensional deformation and sedimentation was produced, related to the opening of the Bay of Biscay (Rat, 1988; García-Modéjar, 1996).

The North Pyrenean Fault (NPF), situated between the PAZ and NPZ, is a major tectonic structure running east–west along the whole Pyrenean range and interpreted as the surface expression of the Mesozoic plate boundary between Iberia and Europe (Choukroune, 1992). However, the NPF can not be seen as a single linear feature; it includes a multiplicity of segments which are not necessarily E–W oriented, fault-bounded blocks undergoing differential rotations, pull-apart basins and basinal areas where lower crustal and upper mantle bodies where emplaced, conforming a domain of several tens of kilometres wide (Choukroune, 1992; Larrasoaña et al., 2003a). Different geophysical studies since the 80s reported a complex deep structure and important structural variations associated with the transition between the PAZ and NPZ domains (Gallart et al., 1981; ECORS Pyrenean Team, 1988; Daignières et al., 1994; Souriau and Granet, 1995; Pous et al., 1995). They revealed the existence of a 10–15 km Moho jump beneath the trace of the NPF, which pointed to a major role for this structure in controlling the northward underthrusting of the Iberian plate beneath the thinner European plate. However, it is interpreted nowadays that this structure is passively deformed during the compressional stage, and the underthrusting of the Iberian crust begins further south (Choukroune et al., 1990; Muñoz, 1992; Muñoz, 2002). The trace of the NPF vanishes towards the western end of the Pyrenean range. The PAZ crops out here as a series of individual massifs (Igountce, Mendibelza, Labourd, Aldudes-Quinto Real and Cinco Villas), known as the Paleozoic Basque Massifs. Paleomagnetic data (Van der Voo and Boessenkool, 1973; Schott and Peres, 1988; Larrasoaña et al., 2003a) suggest that the structural boundary associated to the NPF is prolonged westward through the Basque–Cantabrian basin along the Leiza Fault (LF). The LF is a steeply dipping E–W trending structure that crops out to the south of the Cinco Villas massif. The fault zone varies between 30 and 500 m and is marked by a wide range of lower crust and upper mantle rocks

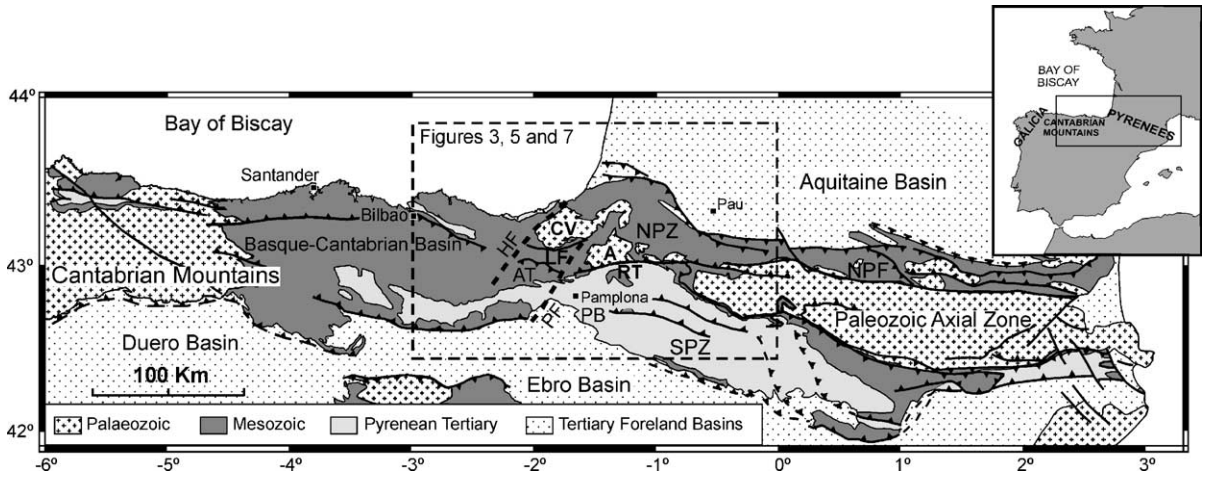

Fig. 1. Tectonic map of the Pyrenean–Cantabrian chain (modified from Pedreira et al., 2003). NPF: North Pyrenean Fault. NPZ: North Pyrenean Zone. SPZ: South Pyrenean Zone. RT: Roncesvalles Thrust. LF: Leiza Fault. PF: Pamplona Fault. HF: Hendaya Fault. AT: Aralar Thrust. PB: Pamplona Basin. CV: Cinco Villas Massif. A: Aldudes Massif.

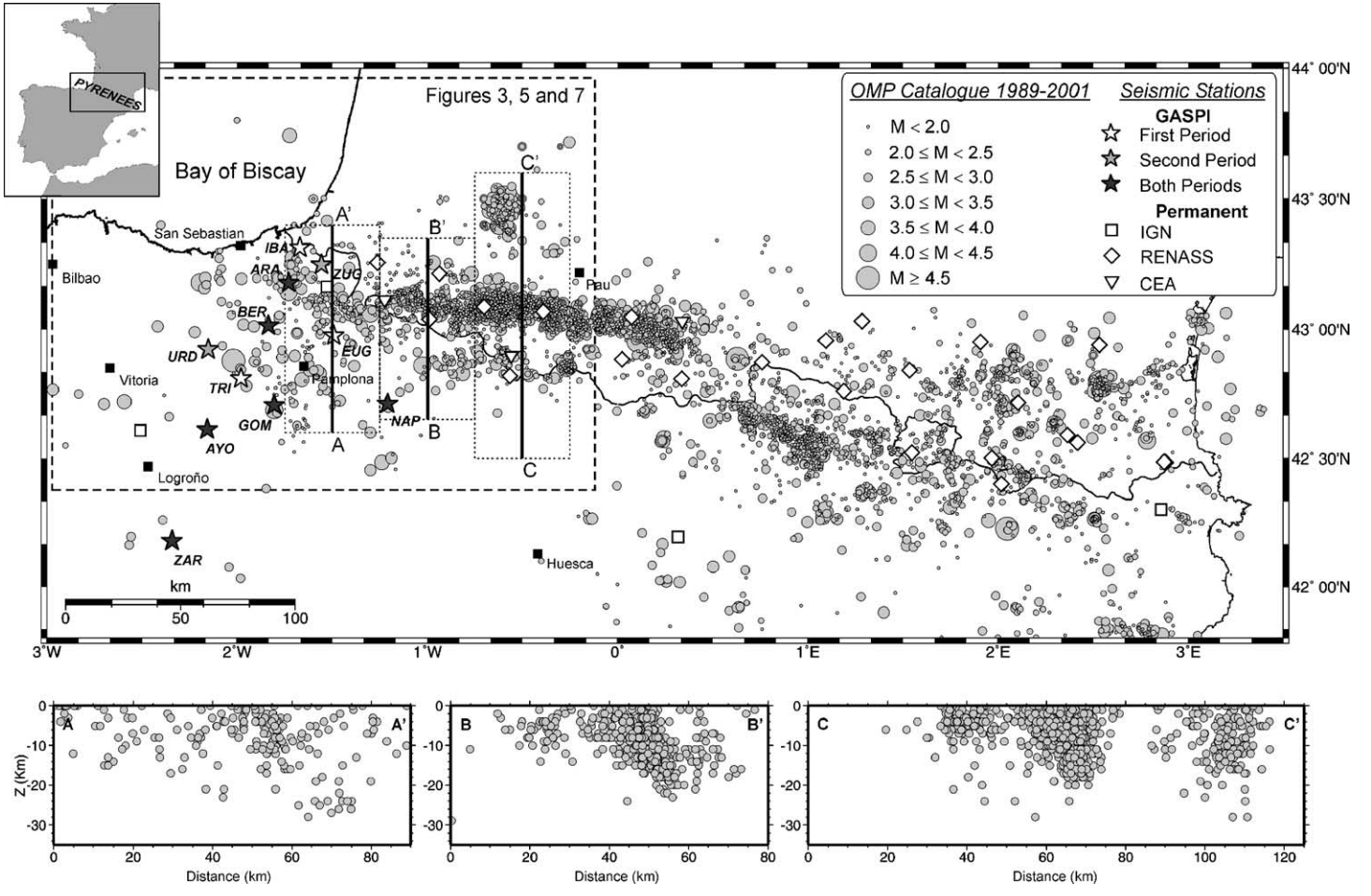

Fig. 2. Epicentral location of the earthquakes reported by the Observatoire Midi-Pyrénées (OMP) catalogue from 1989 to 2001, and three N–S cross-sections showing the northward dipping of the seismicity of the western part of the Pyrenees. The GASPI stations (stars) are shown in different grey intensities to reflect the sites occupied during the different periods. The IGN, RENASS and CEA stations are also shown.

(known in the literature as the 'Nappe des Marbres') such as peridotites, granulites, migmatites and Cretaceous metamorphic rocks similar to those related to the NPF (Rat, 1988; Martínez-Torres, 1989; Mendia and Gil-Ibarguchi, 1991; Faci et al., 1997; Mathey et al., 1999). Martínez-Torres (1989) and Faci et al. (1997) suggest that the LF shows a strike-slip component developed at least over 10–15 km depth, and the absence of Albian and more recent materials in the fault zone suggests that it is a pre-Albian structure.

The Pamplona Fault (PF), also known as Estella Fault, is a Late-Variscan, NE–SW striking vertical deep structure that runs from the Paleozoic Basque Massifs to the Ebro Basin. The fault is at least 125 km long (Turner, 1996), although it appears partially buried by Mesozoic and Tertiary deposits. In its central segment, inside the Pamplona basin, a line of diapirs of Triassic salt follows the fault trace (Martínez-Torres, 1989; Turner, 1996; Faci et al., 1997). The PF played an important role in controlling the Mesozoic and Tertiary sedimentation. In Cretaceous times, it moved only vertically, separating subsiding basins in the west from a more stable area in the east (Rat, 1988). During the Late Eocene this situation was inverted and the subsidence was produced in the eastern side (Faci et al., 1997). During the compressional stage, it has been classically interpreted as a major strike-slip fault with either sinistral (Engeser and Schwentke, 1986; Rat, 1988; Faci et al., 1997; Pedreira et al., 2003), dextral (Müller and Rodgers, 1977; Turner, 1996) or combined (Martínez-Torres, 1989) sense of movement. More recently, the absence of significant paleomagnetic rotation around the fault has supported a new interpretation of the Pamplona fault as a hanging-wall drop fault resulting from variations of the geometry and thickness of Mesozoic sequences on both sides of the fault (Larrasoaña et al., 2003b; Vergés, 2003).

The Hendaya Fault (HF) is another basement structure, also oriented NE–SW, which marks the westernmost edge of the Basque massifs. As the PF, it was active during the N–S to NNW–SSE Alpine compressional regime, probably producing left-lateral displacements that blended the cartographic traces of the Basque–Cantabrian region (Pedreira et al., 2003). The surface tracing of the HF is lost under the Cretaceous and Tertiary sediments of the Basque–Cantabrian basin.

In summary, the Hendaya and Pamplona faults are interpreted as deep accidents limiting two different structural zones. On the west side most structures have northward vergence, resulting from the inversion of the Basque–Cantabrian basin, whereas on the Pamplona basin at the eastern side, most important thrusting structures are associated with the continental collision processes that affected the SPZ, and face mainly south (Martínez-Torres, 1989; Turner, 1996).

The Aralar thrust unit is located between the PF and the HF. This unit, approximately 30 km long and up to 10 km wide, is composed of Jurassic and Early Cretaceous carbonated terrains disposed along a general E–W direction and forming a north-verging thrust imbricate. Towards its eastern edge, a NNW–SSE fault with a dextral component crosses the whole structure and the thrust direction changes to the SE, probably affected by the NE–SW Pamplona fault (Martínez-Torres, 1989; Faci et al., 1997).

3. Present tectonic stress

At present, the large-scale stress field in most of Iberia has the same NW–SE compressive trend as the western European province (Müller et al., 1992, 1997; Herraiz et al., 2000; Jabaloy et al., 2002). This primary pattern reflects the stresses generated by the convergence between African and Eurasian plates and the W–E ridge push originated in the middle Atlantic rift (Srivastava et al., 1990; Müller et al., 1997; Herraiz et al., 2000; Jabaloy et al., 2002). However, this stress field is not homogeneous and can show small-scale variations over major geological structures.

Focal mechanisms of Pyrenean earthquakes obtained up to now correspond to events of moderate magnitude, and do not allow to define a homogeneous stress field for the whole Pyrenean range (Nicolas et al., 1990; Delouis et al., 1993; Herraiz et al., 2000; Souriau et al., 2001; Vannucci et al., 2004) (Fig. 3). Focal solutions of earthquakes occurred in the western part of the Pyrenees (Fig. 3) tend to suggest a NNW–SSE to NW–SE direction of maximum stress (Gagnepain et al., 1980; Gagnepain-Beyneix et al., 1982; Nicolas et al., 1990; Delouis et al., 1993; Grandjean et al., 1994; Souriau et al., 2001). Other results coming from analyses of borehole breakouts, microfault populations, and both microstructural and seismological data, suggest a present-day stress field with a NNE–SSW to NE–SW compressive trend for the eastern Pyrenees and northeastern Iberian domain (Jurado and Müller, 1997; Herraiz et al., 2000; Jabaloy et al., 2002).

Studies of paleostress evolution in the Iberian Peninsula (Jabaloy et al., 2002) show that during Pliocene most of thrust faults in Iberia became inactive. During the Quaternary and the present-time the active structures appear to be mainly strike-slip and normal faults (Herraiz et al., 2000; Jabaloy et al., 2002). This fact is

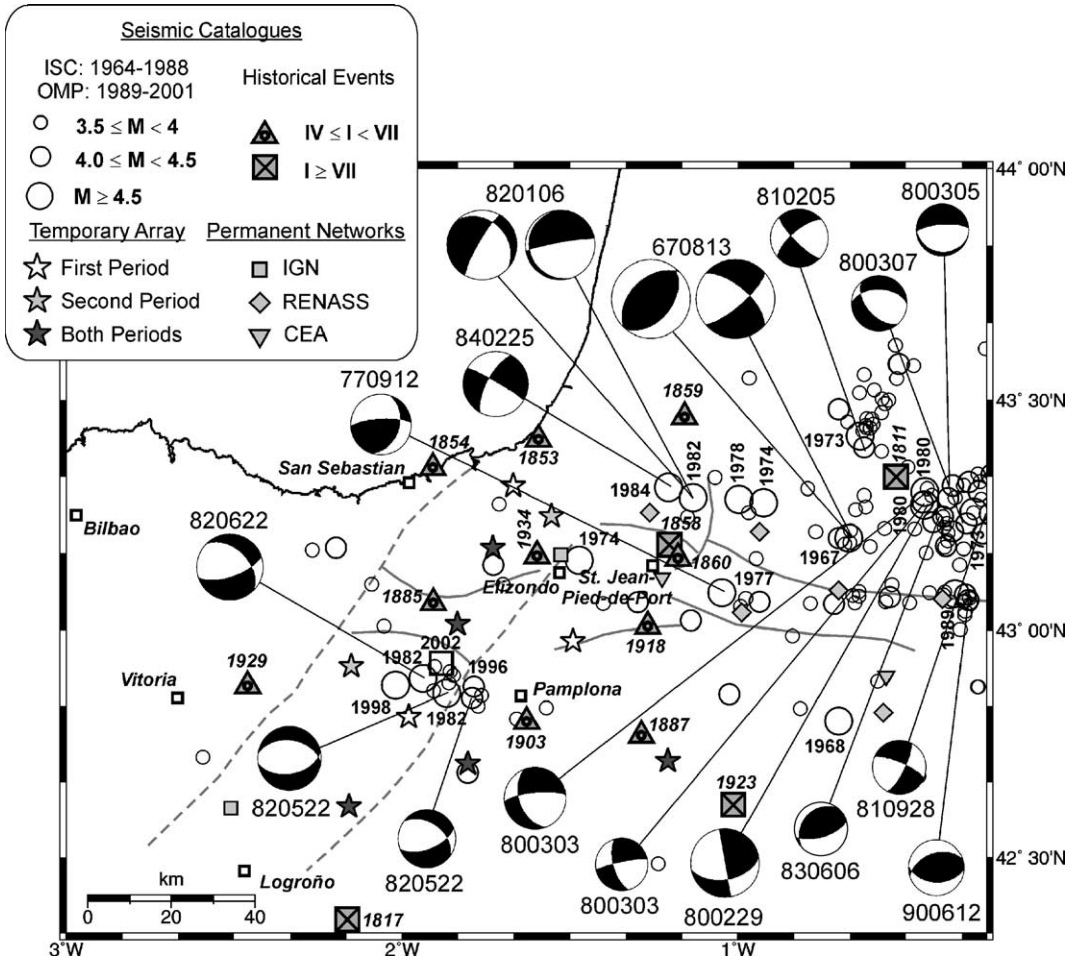

Fig. 3. Seismic events with magnitudes greater than 3.5 included in the International Seismological Centre (ISC) catalogue from 1964 to 1988 and in the OMP catalogue from 1989 to 2001. The major catalogued seismicity in the western Pyrenees is located in an E–W band traditionally related to the NPF. An important seismic focus is also located near the Pamplona region. Focal solutions (lower hemisphere equal-area projection) for the main catalogued events ($M>4.0$) are shown (e.g. Nicolas et al., 1990; Delouis et al., 1993; Souriau et al., 2001; Vannucci et al., 2004). The date for each mechanism (year, month and day) is reported, and its size is proportional to its magnitude. Historical earthquakes with macroseismic intensities between IV and VII (Martínez-Solares and Mezcua, 2003) and greater than VII (OMP catalogue; Souriau et al., 2001) are also shown in the figure.

also evidenced in the earthquakes taking place in the western Pyrenees, which show focal mechanisms with mainly normal fault and strike-slip solutions. Most of the *P*-axes are NW–SE oriented reflecting that the general trend of the maximum stress in this region is NNW–SSE to NW–SE. However, the dips of the *P*-axes range from subhorizontal to subvertical, thus cases of reverse fault are also present in this region (Souriau et al., 2001) (Fig. 3). The NE–SW oriented structures like the PF and HF, and the fault-bounded blocks in the NPF undergoing differential rotations, could be revaluated as possible transverse structures accommodating the N–S compressional regime in the western Pyrenean edge (Larrasoaña et al., 2003a; Pedreira et al., 2003).

4. Previous seismicity results

The historical seismicity of the westernmost Pyrenean region appears to be scarce because only a few intensity values are reported, although it is poorly documented. At most, two seismic activity zones, with reported intensity values between IV and VII, can be distinguished: one of them near the border region, near Elizondo village, on the Paleozoic Basque Massifs and the Roncesvalles thrust, and the second one close to Pamplona city (Martínez-Solares and Mezcua, 2003; Olivera and Gallart, 1987). Three destructive earthquakes with intensity ≥VII are also reported in the study area, between 1811 and 1923, in the Observatoire Midi-Pyrénées (OMP) catalogue (Souriau et al.,

2001) (Fig. 3). The catalogued seismicity in the western Pyrenean range is concentrated on the French side (Figs. 2 and 3). The major activity is focused along an E–W oriented strip 80 km long and 5 to 15 km wide, located between longitudes 0.1° W and 1.3° W, from Lourdes to Saint Jean Pied de Port (Souriau and Pauchet, 1998; Souriau et al., 2001). This activity was traditionally associated to the NPF, the accident assumed to control the tectonic stress release along the western part of the range (Gagnepain et al., 1980; Gallart et al., 1985a; Souriau and Pauchet, 1998). However, analysis of new seismological data shows that this activity can also be related to fault segments which are not necessarily E–W oriented, crossing the NPF zone (Souriau et al., 2001; Rigo et al., 2005). According to these authors, the seismicity at the west-central part of the Pyrenees, between 0.3° E and 0.3° W, can be associated to short structures approximately N–S oriented, separated by aseismic gaps. From 0.5° W to 0.8° W the seismicity is shifted to the north of the NPF, and westward of 0.8° W; it is related to the presence of intrusive blocks (Souriau and Pauchet, 1998; Souriau et al., 2001). In this western region, the hypocentral depths increase westwards down to 20 km, and show a northward dipping (Souriau and Pauchet, 1998) (Fig. 2). The most important events in this zone in the last 40 years were the August 13, 1967 $M=5.5$ earthquake on the Arette region, (Gagnepain et al., 1980), the February 29, 1980 Arudy event, $M=5.1$ (Gagnepain-Beyneix et al., 1982), and the January 6, 1982 Arbailles Massif event, $M=4.8$ (Gallart et al., 1985a) (Fig. 3).

Instrumental catalogues show a moderate and sparse seismicity in the westernmost Pyrenean edge (Fig. 2), where the most outstanding activity is located around the Pamplona region. Between May and June 1982 a seismic crisis produced 28 earthquakes with magnitudes between 2.7 and 4.9 (Olivera and Gallart, 1987). In February 25, 1996 and October 27, 1998 two earthquakes of magnitude 4.4 and 4.9 are reported in the OMP catalogue (Fig. 3). More recently, in February 21, 2002 a magnitude 4.1 earthquake occurred NW of Pamplona, related to the Aralar thrust system (Ruiz et al., submitted for publication).

Concerning the activity close to Elizondo area, a magnitude 4.6 earthquake took place in August 13, 1974 as reported in the International Seismological Centre (ISC) catalogue (Fig. 3). From April to July 1990, 40 seismological stations were set up at the western Pyrenees in the framework of the ECORS-Arzacq project devoted mainly to seismic reflection profiling, and some events were also recorded from the Elizondo region (Grandjean et al., 1994). Recent compilations (Souriau and Pauchet, 1998; Souriau et al., 2001) showed an E–W sparse seismicity in this area, poorly constrained by the low-station coverage.

5. Data acquisition and processing

The seismic network installed in the western Pyrenees area was designed to fulfil the two main aims of the GASPI project, to record a NNE–SSW profile that provides a lithospheric transect across the area reworked during the Alpine orogeny (Díaz et al., 2002, 2003), and to control the present-day seismicity by deploying additional instruments outside the profile. The distribution of the later instruments was planned according to the location of the RENASS, CEA and IGN permanent instruments. The seismic stations were mainly distributed on a NNE–SSW band, about 140 km long and with a mean separation between instruments of approximately 30 km, although it is less than 15–20 km in the northern and central segments. The network runs parallel to the PF, mainly at its western side, and covers both sides of the LF. The RENASS and CEA permanent instruments cover the northern sector, allowing appropriate constrain of the seismicity inside the study area (Fig. 2).

The experiment was carried out in two phases: the first one ran from March to August 1999, and the second one from September 2000 to June 2001 (Table 1). During the second period, most of the first emplacements were reoccupied, and some new sites were added to improve data quality. Up to 9 sites were operated at the same time, using Reftek and Leas-Hathor digital dataloggers, with continuous data recording at a sampling rate of 50 sps, and GPS synchronization. The stations were equipped with Lennartz Le20s and Le5s three-component seismometers, with flat frequency response broadened up to 20 and 5 s, respectively. The seismic network was maintained through periodical visits every month and a half approximately, that include the recovery of the data stored in hard disks devices.

The identification of events was faced using two different but complementary methods: i) events reported by the published catalogues from permanent networks were readily extracted from our database. ii) Detection algorithms based on STA/LTA methods were applied to the raw continuous data. An event was retained whether it triggered over a minimum of 3 different stations in an 8 s interval.

Finally, only local events within the study area were selected from the whole events extracted by these two

Table 1
Location and description of the instruments deployed during the experiment

Station name	Recording periods	Instrument	Latitude (°N)	Longitude (°E)	Height (m)	Station correction (s)
IBA	03/09/99–08/22/99	Reftek	43.3145	−1.6683	800	0.15
EUG	03/11/99–08/23/99	Reftek	42.9760	−1.4915	900	0.16
TRI	03/11/99–08/22/99	Reftek	42.8107	−1.9804	1200	0.22
BER	03/09/99–08/22/99	Reftek	43.0133	−1.8353	810	0.15
	09/13/00–06/26/01	Reftek				
ARA	03/09/99–08/22/99	Reftek	43.1789	−1.7300	415	0.08
	09/15/00–06/26/01	Reftek				
ZAR	06/01/99–07/29/99	Hathor	42.1810	−2.3427	1020	0.19
	09/14/00–06/25/01	Reftek				
GOM	03/10/99–08/22/99	Reftek	42.7072	−1.8042	590	0.11
	09/14/00–06/25/01	Reftek				
NAP	06/01/99–07/27/99	Hathor	42.7125	−1.2077	765	0.14
	09/15/00–06/26/01	Reftek				
AYO	06/02/99–07/29/99	Hathor	42.6125	−2.1576	520	0.09
	09/14/00–06/25/01	Mars88				
URD	10/18/00–06/26/01	Mars88	42.9215	−2.1519	590	0.11
ZUG	09/13/00–06/26/01	Reftek	43.2493	−1.5561	540	0.10

The correction ascribed to each station due to its altitude is reported.

methods. We then compile a complete catalogue containing:

a) Hypocentral relocations of the events previously catalogued by seismological services, using the phase-picking of both temporary and permanent seismic networks.
b) Determinations of events not catalogued previously by any seismological organization.

Phase-picking and seismogram analysis was performed with SAC2000 (Seismic Analysis Code) program (Goldstein and Minner, 1996; Goldstein et al., 2003). First hypocentral determinations were carried out using the inversion program Hypo71 (Lee and Lahr, 1975).

The P-wave velocity model used in the hypocentral inversion is a homogeneous 5 layered structure (Table 2) derived from all the information available for this region, mainly from wide-angle seismic profiles (Gallart et al., 1981; Daignières et al., 1981; Pedreira et al., 2003). A mean Poisson's ratio of 0.25 is assumed to infer the S-wave velocity model. The first layer in the velocity model is an average of the sedimentary cover. Nevertheless, a time correction was ascribed to each station (Table 1) to take into account the topography and velocity model differences, mainly coming from sedimentary thickness variations in both sides of the PF.

Table 2
P-wave velocity model used for hypocentre inversion

Depth Z (km)	V_P (km/s)
0.0	5.5
3.0	6.0
12.5	6.2
22.0	6.7
38.0	8.0

In order to fix the magnitudes for all the earthquakes detected, we first established a local magnitude (M_L) formula, defined as an empirical relationship involving epicentral distance and total signal duration. We use duration magnitude instead of the usual local magnitude derived from S-wave amplitude, because our network was composed of different types of instruments and geophones, with no appropriate calibration in all cases.

We considered a relation of the form (Lee et al., 1972; De Miguel et al., 1988; Samardjieva et al., 1999):

$$M_L = a + b\ \log T + cD$$

where T is the total signal duration in seconds, D is the epicentral distance in kilometres and a, b and c are constants determined statistically. The coefficients of the formula were adjusted in a least-squares analysis using data from 17 events that occurred inside our network, and having known local magnitudes as catalogued by the OMP service. The OMP centre relocates the Pyrenean seismicity, gathering arrival times from IGN, CEA and RENASS and building the most complete catalogue of the Pyrenean region.

This inversion procedure resulted in the following equation, with a correlation coefficient of 88%:

$$M_L = -2.120 + 2.406\ \log T + 0.0023D.$$

In the first stage, a total of 249 events were located. A subsequent analysis led us to reject from the final catalogue earthquakes with high error or location instabilities due to insufficient phase lectures or poor station coverage. Artificial events were also excluded. Blasts can often be distinguished from earthquakes (Street et al., 2002) according to features such as lower frequency content, a well developed dispersive wave train, a large P- to S-wave amplitude and time and location repetition. The mean quality obtained for the hypocentral locations is mainly B or C (Lee and Lahr, 1975), using a mean of 12 observations (first P and/or S arrival time readings), and always ≥ 6 (Appendix 1). The locations obtained have a mean RMS value of 0.10 s, being always lesser than 0.25 s. The mean horizontal and vertical errors are 0.8 and 1.3 km, respectively, being always below 3 and 5 km, respectively.

The final catalogue consists of 179 earthquakes, corresponding to an average rate of 10 events per month, with magnitudes ranging between 0.5 and 3.5 (Appendix 1).

Fig. 4 shows a comparison of the OMP and GASPI catalogues. Up to 106 of the studied events are not included in the final relocations of the OMP service (Fig. 4a). Approximately half of the 179 retained events, 94, are previously uncatalogued earthquakes, not reported by Spanish or French services. Most of these events are located in the central zone of our network, allowing a more accurate seismotectonic control. Also, the relocation of the 85 earthquakes previously catalogued by seismological services, (the French Pyrenean networks reported 74 and the IGN network 52 of them), resulted in clearly improved hypocentral determinations.

Focal mechanisms were also calculated whenever possible (Fig. 5). P-wave polarity was used to derive focal solutions for earthquakes with best azimuthal coverage. Only events with a gap less than 100° and more than 8 P-phase lectures were considered. With these constraints, 10 focal solutions were obtained using FPFIT program (Reasenberg and Oppenheimer, 1985) (Appendix 2; Fig. 6).

In a further step, the HypoDD programme (Waldhauser, 2001), based on a double-difference hypocentre location approach (Waldhauser and Ellsworth, 2000), has been used to relocate the complete catalogue (Fig. 7). The relative location of event pairs in the DD algorithm minimizes the influence of the velocity model, and decreases the errors produced by the use of a one-dimension velocity model, which do not accurately reflect the real 3D structure of the study area.

6. Seismicity results and tectonic implications

Fig. 5 shows the distribution of the seismicity and the focal mechanisms obtained. In the easternmost part of the study area only the most relevant events catalogued by seismological services have been relocated by combining data from temporal and permanent instruments. These earthquakes are appropriately covered by RENASS and CEA Pyrenean Networks and have been extensively studied in previous works (Gagnepain et al., 1980; Gallart et al., 1985a; Grandjean et al., 1994; Souriau and Pauchet, 1998; Souriau et al., 2001). Therefore, the present work was focused on the westernmost edge of the range, where the seismic network joining temporal and permanent stations had its maximum coverage. The results obtained can be discussed with respect to their seismotectonic implications.

6.1. Westward prolongation of the E–W Pyrenean seismicity

At the easternmost zone of the study area, up to 38 earthquakes, with magnitudes between 1.2 and 3.5, previously catalogued by the permanent networks, were relocated (Fig. 4b). These events clearly confirm the general E–W pattern of the seismicity in this Pyrenean zone (Figs. 2 and 5), already proved by the permanent French networks (Souriau and Pauchet, 1998). Focal mechanisms were obtained for three of these earthquakes. They show a strike-slip solution, with one of the nodal planes subvertical and east–west oriented. These solutions agree with those proposed in previous studies (Fig. 3) for the same region (Gallart et al., 1985b; Olivera and Gallart, 1987; Souriau et al., 2001).

The GASPI temporary network allowed to detect a relevant seismic activity in the Basque Massifs region. Up to 54 earthquakes with magnitudes between 0.5 and 3.0 were recorded in this area. These events clearly delineate an E–W distribution along the Leiza fault, thus revealing a westward continuity of the E–W characteristic Pyrenean narrow band of seismicity.

Hypocentral determinations show that this seismicity belt detected in the Cinco Villas Massif (Fig. 5) is distributed on a crustal scale, dipping northward from surface to almost 30 km depth (Fig. 7, cross-section B–B' and Fig. 8), even if events deeper than 20 km correspond to a single aftershock crisis recorded within two days following a 3.0 earthquake occurred at 30 km depth (Appendix 1). Focal mechanisms calculated for two events of this region display a normal fault solu-

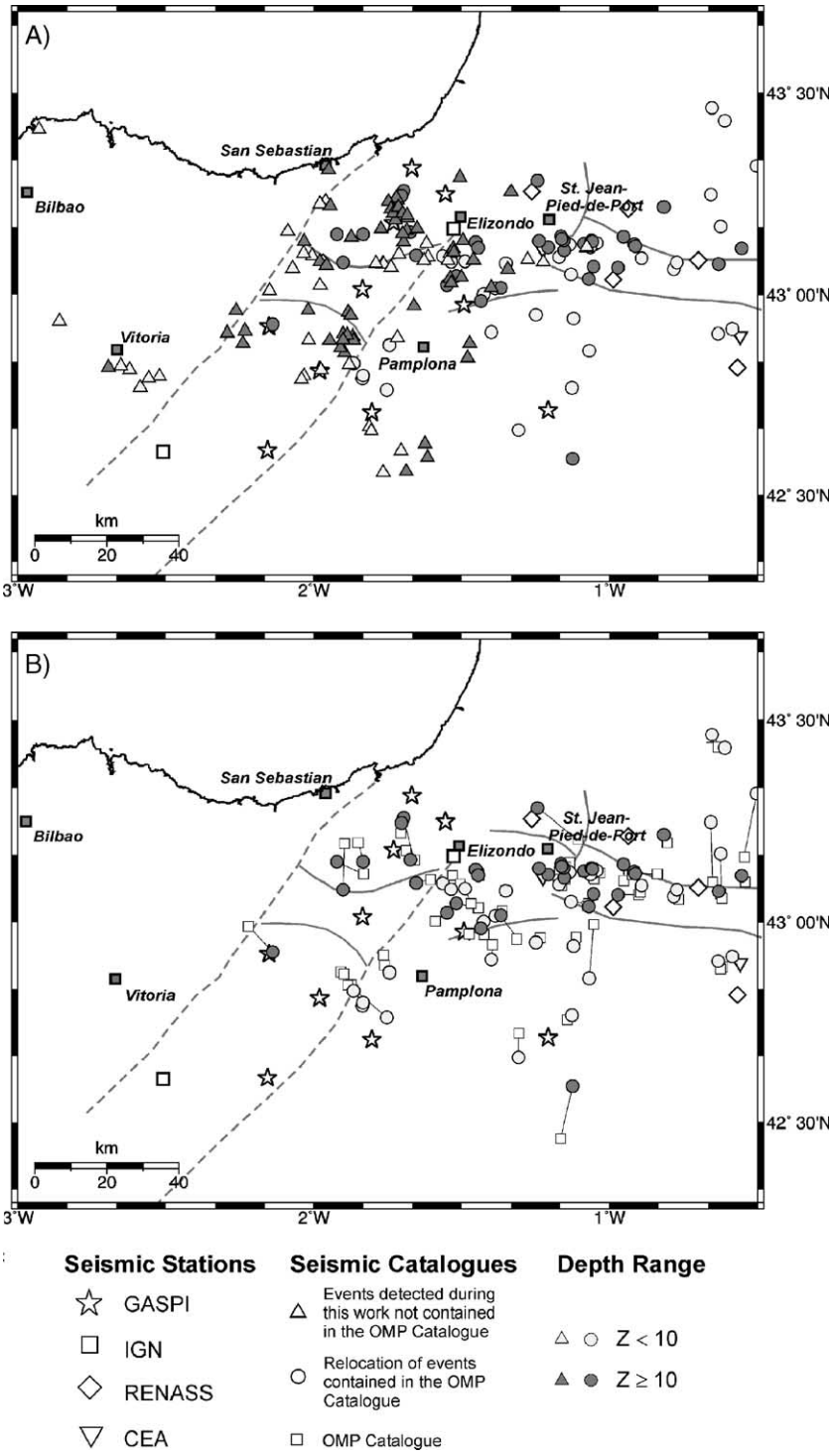

Fig. 4. Catalogue comparisons. A) Grey triangles represent earthquakes found by the detection algorithms applied to the continuous data of the GASPI project, which were not contained in the OMP catalogue (107 events). Grey dots depict the epicentral relocation of events previously catalogued by OMP service, using data from both temporary and permanent networks (72 events). Grey intensities for the triangles and dots of GASPI locations indicate the depth range of the hypocentres. B) Comparison of GASPI and OMP service relocations.

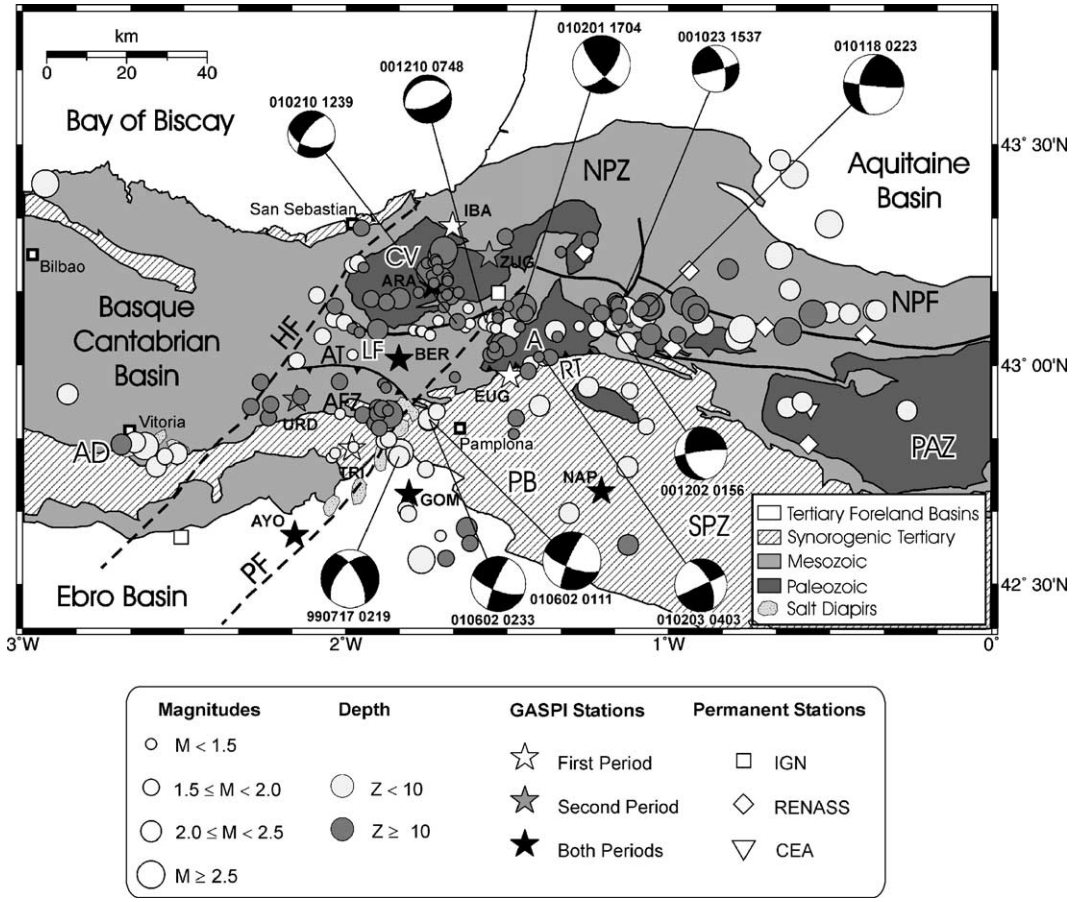

Fig. 5. Schematic tectonic map (modified from Gómez et al., 2002) with the epicentral distribution of all the seismic events located during the two operation periods of the array. The depth range and event magnitude are expressed with different grey intensities and symbol sizes, respectively. Focal mechanisms obtained (lower hemisphere equal-area projection) are also shown. NPF: North Pyrenean Fault. NPZ: North Pyrenean Zone. SPZ: South Pyrenean Zone. PAZ: Paleozoic Axial Zone. LF: Leiza Fault. AT: Aralar Thrust. AFZ: Andia Fault Zone. HF: Hendaya Fault. PF: Pamplona Fault. PB: Pamplona Basin. RT: Roncesvalles Thrust. CV: Cinco Villas Massif. A: Aldudes Massif. AD: Alavese Diapirs.

tions with a small strike-slip component, and one of the nodal planes E–W oriented. This result agrees with the E–W trending of the LF structure, and with solutions depicted from a previous study (Grandjean et al., 1994).

The down-dip distribution of seismicity beneath the LF was poorly constrained from permanent networks (see cross-section A–A' in Fig. 2). We documented that this activity is steeply dipping northwards (cross-section B–B' in Fig. 7), in agreement with the seismicity pattern farther east, in the area well covered by French permanent networks (cross-sections B–B' and C–C' in Fig. 2). In all these sections the seismogenic structure can not be associated to the Alpine plate boundary between Iberia and Europe, as the E–W narrow band of seismicity lies to the North of the main Alpine crustal ramp that promotes the northward underthrusting of the Iberian crust. Although the LF shows a subvertical dipping in the surface (Martínez-Torres, 1989), the alignment of hypocentres imaged it as a north-dipping crustal ramp (Fig. 8). The LF could represent an extensional feature during the Mesozoic rifting, later reactivated as an inverse fault during the Alpine continental collision, promoting the uplift of the Cinco Villas Basque massif. Its present seismic activity as a normal fault evidences crustal readjustments after the shutting down of the orogenic activity.

It is also remarkable that in the transect of Fig. 8 the seismicity associated to the LF seems to reach the base of the crust, even if events deeper than 20 km correspond to a single crisis, while eastwards of the LF the lower limit of the seismicity is found at 15–20 km depth and coincides with the continuation of the north Pyrenean thrust plunging southwards beneath the Axial Zone (Muñoz, 1992, 2002; Teixell, 1998). This suggests possible lateral variations in the structure of the orogen, probably inherited from the geometry of the

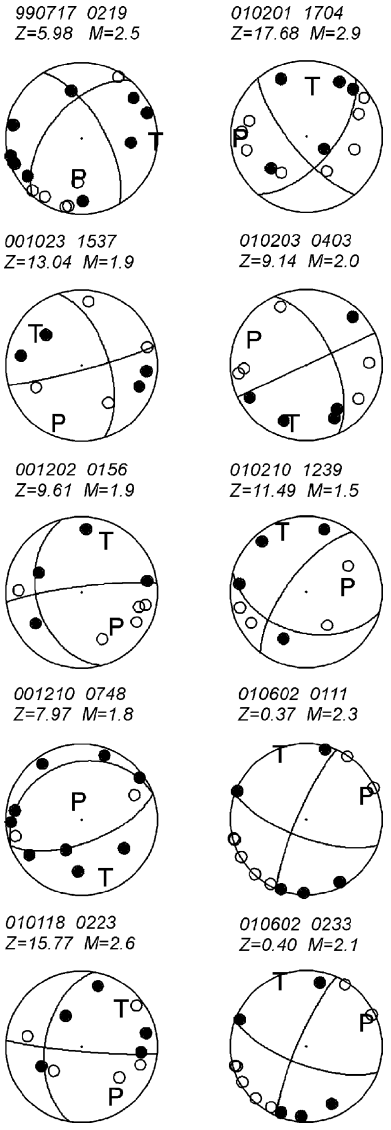

Fig. 6. Fault plane solutions (lower hemisphere equal-area projection) of the 10 studied events. The date (year, month and day), origin time (hour and minute), focal depth in kilometres (Z) and magnitude (*M*) of each mechanism are reported. P and T denote the positions of the *P*- and *T*-axes. Open circles and black dots indicate dilatations and compressions, respectively.

Mesozoic rift system, segmented by oblique structures such as the Pamplona and Hendaya faults. However, further geological fieldwork, geophysical probing and detailed crustal restorations are necessary to clarify the structure along this transect.

These seismotectonic features can also be directly related to the new structural results after seismic profiles (Pedreira et al., 2003) and teleseismic probing (Díaz et al., 2003). These studies revealed that the indentation between European and Iberian crusts is present throughout the northern part of the Iberian Peninsula affected by the Alpine compressional tectonics, and therefore extended the structural image reported in the central Pyrenees since ECORS profiles (Muñoz, 1992; Daignières et al., 1994; Teixell, 1998) to the western Pyrenees and through the transition to the Cantabrian Mountains.

The E–W seismicity belt seems to end at the Hendaya fault (Fig. 5). This structure also marks the end of the metamorphic outcropping associated to the LF. From the coast to almost 40 km to the SW, along the Hendaya fault, 13 earthquakes with magnitudes between 1.5 and 2.0 have been recorded. Such kind of alignment had not been revealed so far, as permanent instruments leave a coverage gap of almost 250° for this area. Our temporary array was closer to the epicentral region, allowing to detect such events. However, 17 months is a rather short observational period and our array was not specifically designed to cover this area. Therefore, to better constrain this westernmost hypocentral zone, additional permanent stations should be deployed in the Basque–Cantabrian basin.

6.2. Seismic activity related to the Pamplona fault

A concentration of seismic events is observed westward from the city of Pamplona. Fig. 5 shows the 24 earthquakes located in this area, with magnitudes between 0.9 and 2.5. A NW–SE cross-section reveals a vertical distribution in depth between 0 to 20 km (Fig. 7, cross-section A–A'). This seismicity is located on the central segment of the PF, at the vicinity of the outcrops of the Pamplona basin salt diapirs and of the so-called Andia Fault Zone (AFZ), a network of shallow faults with EW and NE–SW orientations (Faci et al., 1997; Larrasoaña et al., 2003b). However the hypocentral depths do not favour a simple relationship between all this seismicity and these shallow diapiric structures and faults.

Three focal mechanisms have been calculated for this area. They reveal a normal to subvertical fault solution with strong strike-slip component. All solutions obtained have one nodal plane NNE–SSW oriented, consistent with the PF trending. They also agree with solutions presented in a previous compilation work for the Iberian Peninsula (Herraiz et al., 2000).

Events in the Pamplona cluster seem to propagate from PF to the north–west. A few earthquakes were located between the Pamplona and Hendaya faults with an E–W orientation, and could be related to the Aralar thrust system (Fig. 5). The seismotectonic relevance of this structure, as revealed in recent aftershocks studies

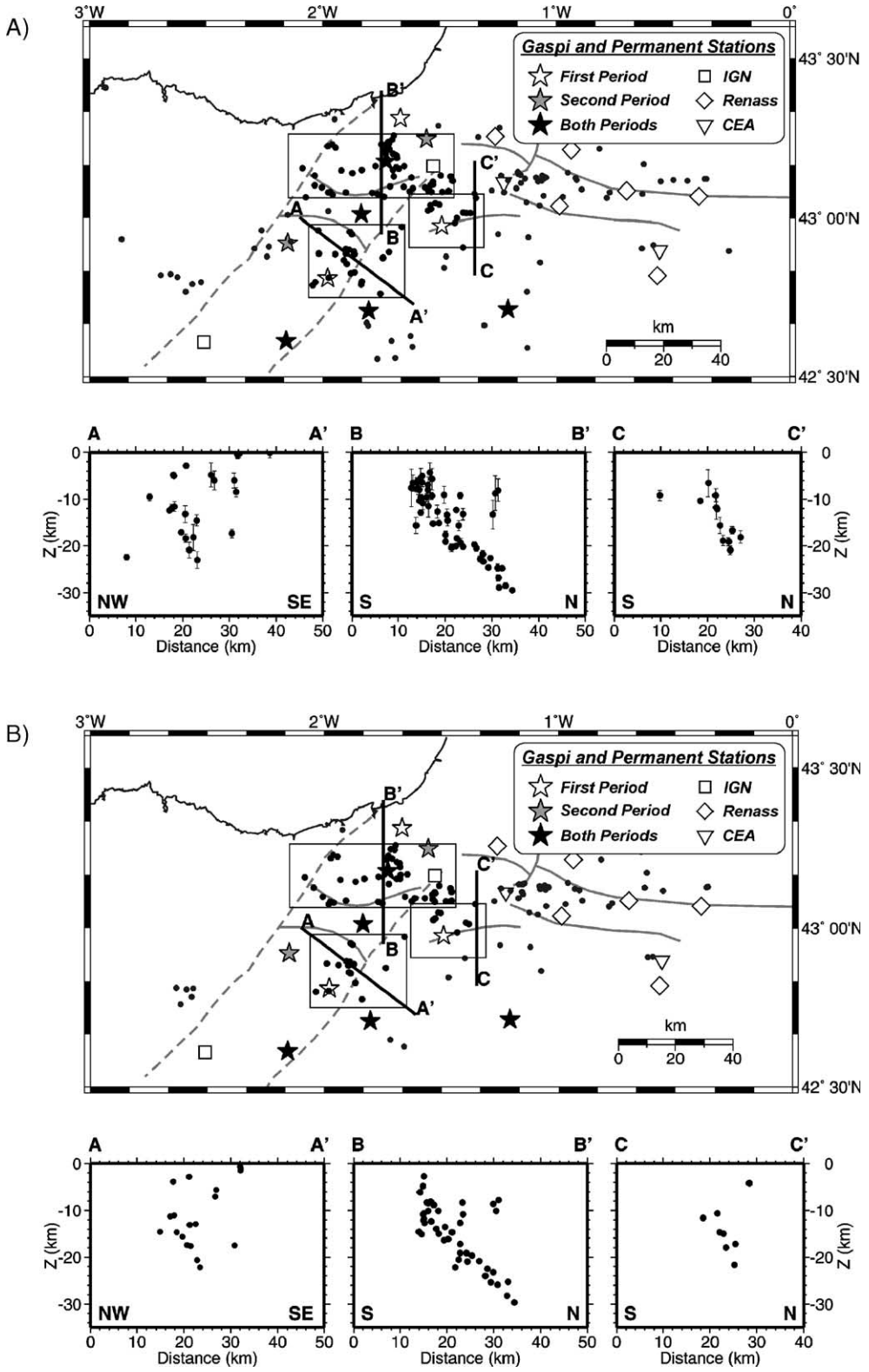

Fig. 7. A) Seismicity distribution in depth along different N–S and NW–SE vertical sections across the major structures, discussed in the text. B) Relocation of the complete catalogue using the double-difference approach. The seismicity distribution in depth is also shown along the same cross-sections as in the previous figure.

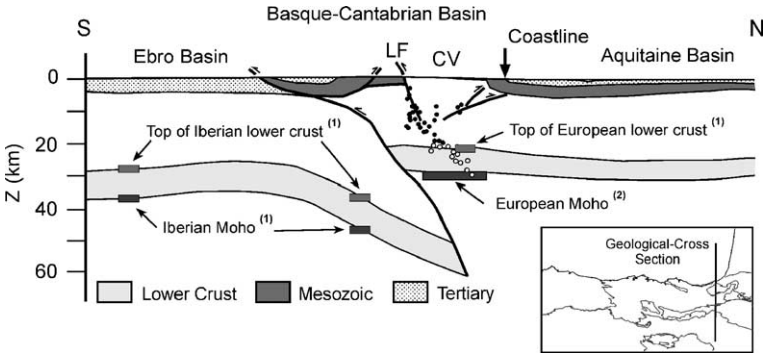

Fig. 8. Cartoon of the crustal structure, derived from seismic and 3D gravity and magnetic modelling (Pedreira, 2004; Pedreira et al., submitted for publication) along the trace of the N–S section B–B' with the earthquake hypocentres superimposed. Constraints on the position of the Moho and the top of the lower crust are marked at the intersection with available seismic refraction and receiver function profiles: (1): Pedreira et al. (2003) and (2): Gallart et al. (1981), Díaz et al. (2003). LF: Leiza Fault. CV: Cinco Villas Massif.

(Ruiz et al., submitted for publication), could not be inferred from the sparse distribution of hypocentres established from permanent networks due to low coverage of stations operating in this area.

The northern segment of the PF, between the salt diapirs and the LF, does not show a remarkable seismic activity (Fig. 5). The PF dies out in the Basque massifs, between Cinco Villas and Aldudes-Quinto Real metamorphic complexes (Turner, 1996), where the seismicity is again present, but widely distributed along an E–W band. This geographical distribution favours a correlation of the seismicity with the E–W Roncesvalles thrust system (RT) that separates the Aldudes massif from the Pamplona basin. This fact is also supported by a focal mechanism derived, that shows a strike-slip solution with one of the nodal planes mainly E–W oriented. However, it must be noted that the maximum concentration of events in this region corresponds to the westernmost part of the RT, close to the PF. On the Aldudes-Quinto Real massif, the hypocentres show a distribution in depth from 5 to 20 km (Fig. 7, cross-section C–C').

6.3. Seismic activity in other south Pyrenean and Basque–Cantabrian zones

About 30 km southward of Pamplona city, a group of 10 events can be seen in Fig. 5. These earthquakes have magnitudes around 1.2 to 2.5, and can be associated to the south Pyrenean frontal thrust crossing this region with E–W direction delineating the contact between Pamplona and Ebro basins.

Southeastward of Vitoria city, 7 events were recorded with magnitudes between 2.0 to 2.5 and depths from 2 to 14 km. These earthquakes can be associated to the line of Alavese salt diapirs. This alignment, parallel to the main structures of the Basque–Cantabrian basin, is the surface expression of a fault system buried beneath Cretaceous and Tertiary sediments, which can be observed in commercial seismic profiles (García-Modéjar, 1996; Cámara, 1997; Gómez et al., 2002). These earthquakes could be related to fault movements or diapiric rising and pushing.

7. Conclusions

New seismic data obtained in the western Pyrenean edge, provide an enhanced image of the seismic activity in this region, poorly constrained from the permanent seismological services monitoring the area. Around 10 events per month were recorded, generally of a moderate to low magnitude. A comparison of catalogues obtained by this temporal network and those provided by the OMP service, which relocates the Pyrenean seismicity joining all the information coming from permanent networks (Fig. 4), shows that approximately half of the events that happened in this period (with magnitudes between 0.5 and 2.5) couldn't be correctly detected and located by these networks.

The new results obtained in this study confirm the important seismic activity on the E–W Pyrenean belt and reveal its westward continuity through the Basque massifs along the Leiza Fault, up to the Hendaya Fault. The LF is manifested as a crustal-scale deep structure, with an important northward dipping seismicity, continuously distributed from surface to almost 30 km depth. Our data reveals also that the Hendaya Fault is a border that seems to mark the termination of the E–W Pyrenean seismicity belt, hence supporting the importance of this fault in the Cenozoic tectonics. A relevant seismic activity associated to the central segment of the PF was also detected. The seismicity is located between

the Aralar thrust and the E–W and NE–SW oriented faults of the AFZ, at the vicinity of saline dome outcrops. Although a direct relation with these structures and the rising movements of the diapirs is not established, the seismicity detected in this area may be explained in terms of relative movements and interactions affecting the whole fault systems. In the northern edge of the PF, events are related to the RT but it must be noted that the maximum activity is again located in the vicinity of the PF. Moreover, some activity has been found in relation to the south Pyrenean frontal thrust, to E–W structures beneath the Pamplona basin and to WNW–ESE trending faults beneath the southern part of the Basque–Cantabrian basin.

The latent seismic activity on a crustal scale evidenced in this work at the western edge of the Pyrenees, presently of low to moderate amplitude but with significant events of magnitude around 5 in past decades, their established relation to tectonic structures playing a major role in the geodynamic evolution of the area, and the lateral extent of the crustal imbrication of the European and Iberian domains are outstanding features to be considered in future studies of seismic hazard and seismotectonics in North Iberia. Monitoring the seismic activity in the transition between the Pyrenees and the Cantabrian Mountains deserves clear improvement, and combination of permanent equipment with deployment of temporary arrays has proved a remarkable efficiency both for seismotectonic and structural purposes.

Acknowledgements

This work was carried out with the support of the GASPI (AMB98-1012) and MARCONI (REN2001-1734) projects from the Spanish MCYT. M.R. and C.L. benefited from a PhD scholarship from the Spanish MCYT. The authors wish to thank the two anonymous reviewers for their constructive comments on this manuscript. Spanish (IGN) and French (OMP, RENASS and CEA) seismological services are also thanked for providing seismic data from their permanent stations.

Appendix A

Hypocentral parameters, obtained with the Hypo71 program, of the seismic events studied during the two operation periods of the array. GAP: largest azimuthal separation in degrees between stations. RMS: root mean square error of time residuals in seconds. ERH: standard error for the epicentre location in kilometres. ERZ: standard error for the focal depth in kilometres. Q: quality of the hypocentre determination indicating the general reliability of the solution. SQD: QS and QD rating. QS is rated by the statistical measure of the solution, and QD according to the station distribution. NO: number of station readings used in locating the earthquake. P and S arrivals for the same station are regarded as 2 readings. DM: epicentral distance in kilometres to the nearest station. (Lee and Lahr, 1975).

Date	Origin time	Latitude (°N)	Longitude (°E)	Depth (km)	Magnitude	GAP (°)	RMS (s)	ERH (km)	ERZ (km)	Q	SQD	NO	DM (km)
1999/03/12	09:54:00.48	43.0762	−0.6312	11.80	2.76	161	0.18	1.0	1.2	C	B|C	13	6
1999/03/14	16:38:42.98	43.0015	−1.4267	6.56	1.86	188	0.06	0.4	2.9	C	B|D	12	32
1999/04/03	03:44:19.67	43.1342	−1.4958	14.58	1.46	214	0.09	0.7	1.2	C	A|D	8	18
1999/04/09	06:19:42.62	43.1273	−1.0858	12.32	1.70	102	0.19	0.8	1.5	B	B|B	14	13
1999/04/11	07:17:28.14	42.7913	−1.8352	8.46	2.19	121	0.11	0.6	1.0	B	A|B	14	10
1999/04/16	12:08:51.45	43.2212	−1.9455	13.29	1.47	242	0.17	2.3	3.1	C	B|D	8	18
1999/04/18	02:46:28.79	43.2483	−0.6577	2.03	2.50	218	0.19	1.3	1.6	C	B|D	17	18
1999/04/21	08:33:57.76	43.3193	−0.5015	8.88	2.64	259	0.20	2.4	2.7	C	B|D	12	29
1999/04/21	23:19:34.59	43.0822	−1.9787	12.88	1.14	280	0.04	0.5	0.5	C	A|D	8	14
1999/04/28	20:25:49.78	43.1102	−1.1532	10.16	1.81	121	0.11	0.5	1.1	B	A|B	13	16
1999/05/03	18:47:45.39	43.2837	−1.2440	18.67	1.74	295	0.02	0.4	0.9	C	A|D	7	35
1999/05/10	02:01:30.28	43.1142	−1.5293	12.66	1.28	195	0.10	0.7	1.4	C	A|D	9	16
1999/05/11	10:14:08.00	42.8957	−1.8683	18.19	1.44	146	0.15	2.9	2.8	C	C|C	6	13
1999/05/13	19:07:43.34	42.9618	−2.0192	22.39	1.58	227	0.07	1.1	0.6	C	B|D	9	16
1999/05/14	00:38:04.07	43.0097	−2.1508	8.01	1.92	261	0.11	1.0	2.9	C	B|D	12	25
1999/05/15	13:48:47.13	43.0937	−1.6142	9.61	1.17	153	0.06	0.3	0.9	B	A|C	8	13
1999/05/23	13:29:04.26	43.1037	−1.5392	9.29	1.51	189	0.04	0.3	0.7	C	A|D	8	15

Appendix 1 (*continued*)

Date	Origin time	Latitude (°N)	Longitude (°E)	Depth (km)	Magnitude	GAP (°)	RMS (s)	ERH (km)	ERZ (km)	Q	SQD	NO	DM (km)
1999/05/24	10:24:57.15	42.8870	−1.8663	14.54	2.50	147	0.09	1.0	1.2	B	A|C	7	13
1999/05/25	12:27:33.25	43.2315	−1.9613	8.07	1.74	247	0.10	0.9	2.4	C	B|D	10	20
1999/05/25	20:57:18.70	43.1348	−1.0617	13.35	2.30	131	0.16	0.8	1.4	B	B|B	18	13
1999/05/26	10:06:58.88	42.8558	−1.8965	23.09	1.70	140	0.23	1.8	1.8	C	B|C	11	9
1999/06/06	21:43:25.75	42.1340	−2.1663	0.28	1.87	126	0.17	0.9	1.8	C	B|C	20	15
1999/06/08	03:41:30.75	42.8958	−0.2617	2.27	2.15	284	0.23	0.8	1.9	C	B|D	21	19
1999/06/08	18:37:01.76	43.1502	−1.9215	20.04	1.71	211	0.13	0.6	0.5	C	A|D	20	16
1999/06/10	07:52:05.11	43.0225	−1.9787	0.87	1.35	200	0.14	0.5	0.7	C	A|D	14	11
1999/06/11	02:08:18.82	43.1442	−0.9515	12.61	3.22	164	0.21	0.8	1.4	C	B|C	26	21
1999/06/11	11:47:57.57	43.1160	−0.5532	10.38	3.51	183	0.23	1.0	0.7	C	B|D	24	12
1999/06/12	03:01:16.07	43.0762	−1.7667	7.78	1.38	155	0.06	0.4	0.7	B	A|C	9	9
1999/06/14	00:39:22.22	43.2557	−1.3337	17.88	1.33	279	0.04	1.0	1.8	C	B|D	6	28
1999/06/14	16:44:41.11	43.4102	−2.9305	5.92	2.50	295	0.06	1.1	1.1	C	B|D	7	99
1999/06/15	11:19:33.92	42.9273	−2.1390	14.16	1.87	181	0.10	0.9	2.1	C	B|D	11	18
1999/06/15	11:27:52.09	43.2910	−1.5055	10.68	1.64	257	0.06	0.9	1.6	C	A|D	7	13
1999/06/15	11:35:46.50	42.9567	−1.8838	12.48	1.46	178	0.08	0.5	0.5	B	A|C	11	7
1999/06/15	23:12:09.09	43.1202	−0.4988	0.34	2.22	306	0.18	1.3	1.0	C	B|D	18	17
1999/06/16	11:00:31.11	42.9022	−1.9013	17.13	1.61	169	0.03	0.3	0.3	B	A|C	9	12
1999/06/18	11:47:50.38	42.8678	−1.9095	20.94	1.77	156	0.19	1.7	1.7	C	B|C	9	9
1999/06/24	02:57:38.87	42.9487	−1.8758	11.60	1.35	173	0.13	1.1	1.1	C	B|C	9	8
1999/06/25	08:55:18.35	43.0418	−3.3445	14.55	2.17	323	0.09	1.3	1.0	C	B|D	9	108
1999/06/25	10:45:41.07	42.9005	−1.8880	18.37	1.60	160	0.05	1.0	0.9	B	A|C	6	13
1999/06/26	18:03:35.10	43.1557	−1.6740	15.68	1.75	141	0.12	0.6	1.1	B	A|C	11	18
1999/06/28	05:20:55.82	43.1640	−1.7735	13.24	1.03	190	0.05	0.5	1.2	C	A|D	6	18
1999/06/28	15:26:12.75	43.1232	−0.3652	8.06	2.34	277	0.17	1.0	0.6	C	B|D	19	6
1999/06/28	20:52:15.74	42.7987	−2.0335	4.82	1.26	275	0.01	0.2	0.1	C	A|D	6	4
1999/07/02	10:46:45.37	42.8883	−1.9013	13.18	1.60	163	0.15	1.1	1.8	C	B|C	9	11
1999/07/06	11:42:30.76	42.2705	−2.5263	12.08	2.03	268	0.15	1.3	1.1	C	B|D	15	18
1999/07/06	21:06:53.32	43.1180	−1.2075	14.22	1.76	240	0.06	0.6	1.4	C	A|D	10	28
1999/07/09	02:01:47.54	43.0852	−1.6287	5.02	0.63	144	0.02	0.1	0.5	B	A|C	7	13
1999/07/09	07:33:19.20	43.1453	−1.1643	11.89	1.79	270	0.04	0.3	0.4	C	A|D	10	33
1999/07/10	04:23:07.05	43.1862	−1.7258	19.72	1.46	173	0.10	0.6	0.6	B	A|C	12	1
1999/07/13	20:33:27.71	42.8130	−1.9762	2.85	1.37	139	0.13	0.7	0.4	B	A|C	10	0
1999/07/15	04:30:38.89	43.1240	−0.3572	2.77	2.42	282	0.24	1.6	1.2	C	B|D	22	7
1999/07/15	12:57:23.95	43.2262	−1.9793	8.78	1.87	237	0.17	1.6	3.7	C	B|D	11	21
1999/07/15	18:15:08.83	43.3102	−1.9510	10.87	1.58	284	0.18	1.5	1.3	C	B|D	13	23
1999/07/16	11:53:26.44	42.8795	−2.2397	13.04	1.69	244	0.09	1.0	2.4	C	B|D	8	22
1999/07/17	02:19:13.20	42.8000	−1.8332	5.98	2.52	83	0.14	0.4	1.6	B	A|B	26	11
1999/07/19	11:24:34.53	42.6288	−1.6250	13.22	2.00	193	0.13	0.8	1.7	C	A|D	10	17
1999/07/20	11:36:25.80	42.9613	−2.2638	13.31	1.71	254	0.09	1.0	2.8	C	B|D	9	28
1999/07/21	11:35:49.00	43.1335	−2.0338	13.41	1.93	249	0.09	0.8	1.3	C	A|D	9	21
1999/07/22	00:10:05.30	42.9940	−3.3942	14.22	2.50	300	0.10	1.4	0.9	C	B|D	9	84
1999/07/25	23:48:24.27	43.0673	−0.9715	21.07	1.87	270	0.09	0.9	1.0	C	A|D	10	44
1999/07/26	19:39:54.48	42.8787	−1.4728	12.71	1.62	166	0.09	0.9	1.0	B	A|C	9	11
1999/07/31	17:17:38.13	43.1335	−1.2372	23.26	1.50	290	0.03	0.7	1.0	C	A|D	7	27
1999/08/01	04:36:49.57	43.0760	−1.7645	6.31	0.78	154	0.03	0.3	0.8	B	A|C	7	9
1999/08/02	00:25:15.98	42.7890	−2.0425	5.10	0.91	279	0.03	0.5	0.3	C	A|D	6	6
1999/08/06	22:29:38.93	43.0738	−1.9577	15.63	0.95	234	0.06	1.8	1.7	C	B|D	7	12
1999/08/08	10:13:16.42	43.0167	−1.3672	11.78	1.94	304	0.10	2.1	2.6	C	B|D	6	11
1999/08/09	04:10:57.88	43.1057	−1.5282	15.16	1.11	232	0.03	0.4	0.5	C	A|D	6	15
1999/08/11	20:49:54.54	41.1880	−2.1200	14.59	2.50	138	0.20	2.4	2.6	C	B|C	16	41
1999/08/17	12:37:11.82	43.1312	−1.6963	19.14	1.22	163	0.05	0.9	0.5	B	A|C	6	6
1999/08/18	12:19:28.29	42.5945	−1.6152	12.48	1.96	295	0.11	1.1	0.9	C	B|D	9	20
1999/08/19	11:05:48.55	42.5597	−1.6888	13.65	1.97	300	0.12	2.0	2.5	C	B|D	7	19
1999/08/20	10:41:20.19	42.6120	−1.7057	1.09	1.19	316	0.05	1.2	1.1	C	B|D	6	13
2000/09/15	12:08:24.10	42.7978	−2.5225	9.87	2.17	249	0.07	1.1	3.6	C	B|D	8	36
2000/09/16	22:16:57.42	42.0892	−2.2485	6.29	2.47	266	0.15	1.1	1.1	C	B|D	17	13
2000/09/18	01:22:50.46	42.2345	−2.3303	2.32	1.85	189	0.07	2.5	4.7	C	B|D	11	6

(continued on next page)

Appendix 1 (*continued*)

Date	Origin time	Latitude (°N)	Longitude (°E)	Depth (km)	Magnitude	GAP (°)	RMS (s)	ERH (km)	ERZ (km)	Q	SQD	NO	DM (km)
2000/09/21	00:45:10.83	43.4640	−0.6543	5.99	2.00	281	0.11	0.8	1.2	C	A|D	11	63
2000/09/21	17:35:31.10	43.1250	−1.1353	5.76	2.75	164	0.14	0.5	1.7	B	A|C	16	32
2000/09/25	06:27:11.67	43.0818	−1.2233	9.82	1.52	234	0.03	0.6	1.6	C	A|D	6	33
2000/09/26	11:17:21.82	43.1427	−1.8733	20.41	1.76	252	0.12	1.1	0.8	C	B|D	10	12
2000/09/29	13:44:01.32	42.7693	−2.5872	9.63	2.10	254	0.17	1.2	2.0	C	B|D	12	39
2000/10/04	23:43:12.59	43.0705	−1.0540	12.10	2.07	111	0.10	0.4	1.0	B	A|B	14	19
2000/10/15	07:34:26.10	42.9340	−2.8617	3.96	2.43	293	0.10	0.9	0.6	C	A|D	13	46
2000/10/21	06:18:35.58	43.0637	−1.3440	18.13	1.06	204	0.06	0.9	1.3	C	A|D	6	27
2000/10/21	13:03:11.26	43.0878	−1.2762	7.59	1.15	100	0.07	0.4	2.0	B	A|C	11	19
2000/10/23	15:37:34.37	43.1355	−1.1550	13.04	1.90	97	0.13	0.6	1.0	B	A|B	16	16
2000/10/27	14:16:52.81	42.9047	−2.2932	10.74	1.94	298	0.09	0.8	0.9	C	A|D	10	12
2000/10/29	17:32:27.81	42.8430	−1.4797	16.80	1.42	131	0.11	0.6	2.0	B	A|B	10	27
2000/10/29	19:36:10.75	42.9722	−1.6617	17.36	1.41	112	0.07	0.4	0.9	B	A|B	10	15
2000/11/03	18:05:30.52	43.0792	−1.7897	8.05	0.54	176	0.05	1.2	0.9	C	B|C	6	9
2000/11/05	07:13:27.71	43.2178	−0.8158	12.45	2.15	231	0.21	1.2	1.1	C	B|D	13	17
2000/11/10	04:29:50.48	43.1260	−0.9175	15.98	2.71	161	0.13	0.5	0.6	B	A|C	20	11
2000/11/13	21:36:44.57	42.7630	−1.7528	0.11	1.58	120	0.08	0.4	1.0	B	A|C	10	28
2000/11/14	04:17:34.21	42.9153	−0.5847	5.55	2.06	158	0.18	1.1	1.3	C	B|C	17	3
2000/11/14	14:43:00.72	42.8148	−2.6228	7.35	2.50	259	0.10	0.6	1.1	C	A|D	14	40
2000/11/25	05:04:34.53	43.0853	−1.5470	6.47	1.40	148	0.02	0.2	0.9	B	A|C	8	18
2000/11/27	13:18:53.27	43.0405	−1.5398	19.16	1.46	188	0.04	0.5	0.9	C	A|D	6	22
2000/11/30	14:13:45.35	42.8195	−2.6955	13.99	2.18	265	0.06	0.7	0.9	C	A|D	8	73
2000/12/02	01:56:05.00	43.0942	−1.1703	9.61	1.94	78	0.13	0.4	1.2	B	A|B	21	16
2000/12/10	07:48:46.77	43.0967	−1.5638	7.97	1.82	59	0.16	0.5	1.5	B	B|B	21	8
2000/12/13	16:23:42.03	43.0680	−1.7390	6.53	1.09	196	0.04	1.3	1.7	C	B|D	6	10
2000/12/15	06:41:45.84	43.0808	−1.9012	10.39	2.33	212	0.14	0.7	0.5	C	A|D	19	9
2000/12/19	13:27:40.38	42.8868	−1.9470	11.90	1.64	239	0.07	0.7	0.8	C	A|D	8	16
2000/12/22	15:46:18.36	42.8238	−2.6535	9.50	2.47	262	0.07	0.4	0.5	C	A|D	12	47
2001/01/04	21:32:00.18	43.0637	−0.7835	6.11	3.02	107	0.09	0.4	0.8	B	A|B	18	7
2001/01/06	06:56:12.98	43.1247	−1.0520	6.52	1.51	93	0.05	0.2	0.6	B	A|B	13	11
2001/01/14	00:42:57.92	43.0908	−0.8923	4.60	2.39	151	0.08	0.3	0.7	B	A|C	17	10
2001/01/14	12:02:47.30	42.8297	−1.8665	6.01	1.98	121	0.18	0.6	2.0	C	B|C	18	15
2001/01/14	23:03:52.01	42.8267	−1.8808	4.81	1.60	161	0.12	0.6	2.6	C	B|C	10	15
2001/01/18	02:23:44.66	43.1320	−1.0578	15.77	2.63	98	0.20	0.7	1.4	B	B|B	19	12
2001/01/18	21:35:58.71	43.1705	−0.6247	6.31	2.00	201	0.12	0.6	1.1	C	A|D	14	11
2001/01/22	14:19:59.72	43.0812	−0.7715	8.93	2.62	128	0.10	0.6	1.3	B	A|B	9	6
2001/01/24	00:40:22.80	43.0783	−1.3512	4.51	2.38	140	0.09	0.3	4.1	C	B|C	13	17
2001/01/28	14:02:55.20	42.0020	−2.2427	7.86	2.05	290	0.08	0.8	1.1	C	A|D	9	22
2001/02/01	17:04:16.56	43.1308	−1.4525	17.68	2.86	81	0.17	0.6	0.8	B	B|A	24	7
2001/02/01	17:26:14.03	43.1172	−1.4445	15.13	1.93	76	0.10	0.3	0.5	A	A|A	22	9
2001/02/02	23:44:15.35	41.9942	−2.2547	10.80	2.49	168	0.18	1.2	1.0	C	B|C	25	22
2001/02/03	00:08:16.58	43.1205	−0.9130	12.82	1.92	218	0.08	0.4	0.4	C	A|D	15	11
2001/02/03	03:24:34.24	43.0182	−1.4008	12.12	1.45	181	0.02	0.2	0.6	C	A|D	8	29
2001/02/03	04:03:49.62	43.0157	−1.3852	9.14	1.95	71	0.14	0.4	1.4	B	A|C	20	20
2001/02/05	16:44:51.27	43.0967	−2.0048	6.91	1.70	266	0.09	0.9	1.7	C	A|D	10	16
2001/02/10	12:39:42.95	43.0978	−1.6545	11.49	1.52	89	0.20	1.2	2.3	B	B|A	12	11
2001/02/12	02:52:24.86	42.9853	−1.4348	10.31	1.70	71	0.05	0.2	0.5	B	A|C	16	31
2001/02/12	04:01:40.67	42.9073	−1.4002	9.19	2.13	80	0.10	0.3	1.1	B	A|C	19	27
2001/02/14	19:23:48.10	42.9405	−1.1210	8.14	1.75	131	0.07	0.3	1.0	B	A|B	13	15
2001/02/15	11:30:32.73	43.1580	−2.0887	9.21	1.86	282	0.08	0.5	0.7	C	A|D	12	26
2001/02/19	01:45:43.61	43.0823	−1.9682	9.55	1.17	294	0.05	0.7	0.6	C	A|D	8	13
2001/02/23	03:18:17.57	43.1508	−1.8337	12.33	2.09	202	0.07	0.5	0.4	C	A|D	13	25
2001/02/23	11:16:10.82	42.5562	−1.7662	9.15	2.51	280	0.11	1.5	2.9	C	B|D	7	17
2001/02/23	13:33:35.74	43.0433	−1.5008	20.96	2.02	202	0.05	0.5	0.9	C	A|D	8	23
2001/03/07	00:35:53.93	42.7683	−1.1268	9.07	2.41	154	0.14	0.5	1.3	B	A|C	21	9
2001/03/20	13:36:42.50	43.0477	−1.5190	16.66	2.12	149	0.08	0.4	0.8	B	A|C	11	13
2001/03/22	15:09:42.20	42.9103	−2.2327	10.23	1.97	200	0.08	0.7	2.4	C	B|D	10	34

Appendix 1 (*continued*)

Date	Origin time	Latitude (°N)	Longitude (°E)	Depth (km)	Magnitude	GAP (°)	RMS (s)	ERH (km)	ERZ (km)	Q	SQD	NO	DM (km)
2001/03/23	13:26:43.80	43.0233	−1.5505	15.59	1.79	142	0.08	0.6	1.7	B	A|C	8	23
2001/03/23	20:43:26.38	43.1282	−1.0438	6.24	2.32	94	0.10	0.3	1.2	B	A|B	18	11
2001/03/23	22:07:36.98	43.1177	−1.0642	2.39	1.81	91	0.11	0.5	0.9	B	A|C	17	11
2001/03/23	22:42:06.40	43.4315	−0.6108	9.21	2.74	261	0.13	0.8	1.9	C	A|D	20	36
2001/03/24	02:48:17.00	43.1155	−1.0782	2.84	2.50	129	0.06	0.6	0.9	B	A|C	7	11
2001/03/25	04:30:34.72	43.1165	−0.4395	0.14	2.14	277	0.14	1.0	1.0	C	B|D	13	21
2001/03/25	20:44:49.07	43.1187	−1.0777	1.09	1.27	130	0.04	0.3	0.8	B	A|C	8	12
2001/03/26	00:12:50.99	42.6712	−1.8127	6.40	1.76	272	0.06	0.9	0.4	C	A|D	8	4
2001/04/04	05:07:04.82	42.6612	−1.8062	7.55	1.97	273	0.07	0.7	0.5	C	A|D	9	5
2001/04/08	09:42:34.85	42.8605	−1.0690	8.84	1.76	164	0.08	0.5	1.5	B	A|C	8	20
2001/04/11	13:55:17.62	42.9038	−0.6333	1.89	2.28	150	0.17	0.9	1.3	C	B|C	15	6
2001/04/14	09:13:58.27	43.1283	−1.6198	9.07	1.16	213	0.05	1.8	1.8	C	B|D	6	11
2001/04/18	11:09:25.61	43.0293	−1.5370	18.87	1.86	123	0.08	0.4	1.1	B	A|B	12	23
2001/04/18	13:21:23.62	42.7917	−2.5592	1.87	1.96	252	0.11	0.9	1.9	C	A|D	17	38
2001/04/19	11:44:37.08	43.0652	−2.0722	7.59	1.74	316	0.05	1.6	4.0	C	B|D	6	20
2001/04/24	14:06:18.90	42.8885	−2.0185	9.52	1.17	257	0.05	0.5	0.8	C	A|D	8	20
2001/04/28	04:57:59.59	42.6627	−1.3090	0.26	2.00	171	0.16	0.6	1.1	C	B|C	15	10
2001/04/28	12:52:13.13	43.2595	−1.6960	29.47	3.01	228	0.09	0.6	0.4	C	A|D	20	9
2001/04/28	13:00:29.32	43.2325	−1.7283	26.89	0.88	256	0.08	0.9	0.7	C	A|D	8	6
2001/04/28	13:03:49.31	43.2343	−1.7178	28.93	1.25	241	0.06	1.1	0.6	C	B|D	7	6
2001/04/28	13:43:16.92	43.2395	−1.7207	24.86	1.21	244	0.06	0.6	0.4	C	A|D	10	7
2001/04/28	13:51:22.40	43.2313	−1.7480	24.72	0.83	258	0.06	1.5	0.8	C	B|D	6	6
2001/04/28	14:19:03.75	43.2465	−1.7030	28.55	2.86	225	0.15	0.8	0.6	C	B|D	21	8
2001/04/28	14:21:40.04	43.2125	−1.7393	24.60	2.50	249	0.02	0.2	0.2	C	A|D	8	4
2001/04/28	14:37:15.40	43.2032	−1.7328	23.39	0.46	244	0.02	0.5	0.3	C	A|D	6	3
2001/04/28	14:44:42.72	43.2167	−1.7145	22.67	0.77	238	0.05	0.7	0.5	C	A|D	8	4
2001/04/28	15:13:58.49	43.1600	−1.6865	19.31	1.37	105	0.09	0.7	0.9	B	A|B	9	4
2001/04/28	15:23:20.40	43.2022	−1.6998	21.75	1.62	202	0.09	1.1	0.7	C	B|D	9	3
2001/04/28	15:25:20.62	43.1905	−1.6835	20.52	1.06	166	0.06	0.6	0.6	B	A|C	8	4
2001/04/28	15:50:02.08	43.1517	−1.7000	18.36	1.01	178	0.04	0.4	0.4	B	A|C	8	4
2001/04/29	08:18:11.65	43.1642	−1.6510	20.20	0.97	114	0.05	0.5	0.5	B	A|B	8	7
2001/04/29	11:32:15.32	43.1972	−1.6850	22.79	1.25	180	0.06	0.7	0.6	B	A|C	8	4
2001/05/04	19:57:37.92	42.1018	−2.3102	2.08	2.10	172	0.12	0.8	0.9	B	A|C	13	9
2001/05/11	02:54:51.58	43.0832	−1.4883	9.87	2.09	167	0.06	0.4	0.8	B	A|C	8	19
2001/05/18	20:39:10.90	43.1383	−1.1618	12.11	1.61	97	0.09	0.4	0.9	B	A|B	13	15
2001/05/22	20:26:27.63	43.0397	−1.0710	16.66	2.35	86	0.18	0.7	1.5	B	B|A	17	7
2001/05/22	22:53:41.05	43.0505	−1.1297	5.48	2.02	115	0.08	0.4	1.2	B	A|C	12	12
2001/06/01	10:41:27.89	43.1037	−2.0358	5.72	1.80	234	0.08	0.5	2.3	C	B|D	15	19
2001/06/02	01:11:09.21	42.8765	−1.7435	0.37	2.32	88	0.16	0.3	0.8	C	B|C	25	17
2001/06/02	01:19:48.27	42.8935	−1.7182	0.26	1.88	110	0.10	0.4	0.9	B	A|C	11	16
2001/06/02	02:33:23.81	42.8742	−1.7437	0.40	2.11	88	0.15	0.4	0.9	B	A|C	22	17
2001/06/04	17:57:53.10	42.9498	−1.2492	6.35	2.26	106	0.10	0.4	3.1	C	B|C	14	23
2001/06/05	08:22:25.25	43.0825	−1.5352	5.51	1.18	152	0.04	0.3	2.2	C	B|C	8	19
2001/06/10	07:23:56.84	43.1003	−1.7128	4.27	1.02	162	0.06	0.8	2.1	C	B|C	7	9
2001/06/11	21:43:24.64	43.0863	−1.4608	10.84	1.31	177	0.09	0.7	1.4	B	A|C	9	20
2001/06/16	05:26:46.89	42.5908	−1.1248	11.16	2.26	97	0.11	0.9	2.3	B	B|B	11	15
2001/06/17	00:24:24.65	42.1233	−2.6172	9.20	3.15	265	0.09	0.6	0.4	C	A|D	17	24

Appendix B

Focal solutions obtained. FM: number of polarities used in the inversion. The strike (Strk) and dip (Dip) angles for each plane, as well as the azimuth (Azm) and plunge (Plng) angles of the *P*- and *T*-axes, are reported. All the angles expressed in degrees.

Date	Origin time	Latitude (°N)	Longitude (°E)	Depth (km)	Mag	FM	Plane 1		Plane 2		*P*-axis		*T*-axis	
							Strk	Dip	Strk	Dip	Azm	Plng	Azm	Plng
1999/07/17	02:19:13.20	42.8000	−1.8332	5.98	2.5	16	330	65	220	54	190	45	93	6
2000/10/23	15:37:34.37	43.1355	−1.1550	13.04	1.9	8	75	85	342	60	205	17	303	24
2000/12/02	01:56:05.00	43.0942	−1.1703	9.61	1.9	9	165	40	263	84	138	38	23	28
2000/12/10	07:48:46.77	43.0967	−1.5638	7.97	1.8	11	70	65	250	25	340	70	160	20
2001/01/18	02:23:44.66	43.1320	−1.0578	15.77	2.6	10	95	85	189	50	149	23	44	31
2001/02/01	17:04:16.56	43.1308	−1.4525	17.68	2.9	13	40	60	140	73	268	8	4	34
2001/02/03	04:03:49.62	43.0157	−1.3852	9.14	2.0	10	65	90	335	60	294	21	196	21
2001/02/10	12:39:42.95	43.0978	−1.6545	11.49	1.5	8	105	45	217	69	83	49	336	14
2001/06/02	01:11:09.21	42.8765	−1.7435	0.37	2.3	12	110	70	203	81	68	21	335	7
2001/06/02	02:33:23.81	42.8742	−1.7437	0.40	2.1	12	110	70	203	81	68	21	335	7

References

Alonso, J.L., Pulgar, J.A., García-Ramos, J.C., Barba, P., 1996. Tertiary basins and Alpine tectonics in the Cantabrian mountains (NW Spain). In: Friend, P.F., Dabrio, C.J. (Eds.), Tertiary basins of Spain: The Stratrigraphic Record of Crustal Kinematics. Cambridge University Press, Cambridge, pp. 214–227.

Cámara, P., 1997. The Basque–Cantabrian basin's Mesozoic tectono-sedimentary evolution. Mém. Soc. Gèol. Fr. 171, 187–191.

Choukroune, P., 1992. Tectonic evolution of the Pyrenees. Annu. Rev. Earth Planet. Sci. 20, 143–158.

Choukroune, P., Pinet, B., Roure, F., Cazes, M., 1990. Major Hercinian thrusts along the ECORS Pyrenees and Biscay lines. Bull. Soc. Geol. Fr. 8 (VI(2)), 313–320.

Daignières, M., Gallart, J., Banda, E., 1981. Lateral variation of the crust in the north Pyrenean zone. Ann. Geophys. 37 (3), 435–456.

Daignières, M., Séguret, M., ECORS team, 1994. The Arzacq–western Pyrenees ECORS deep seismic profile. Publ. Eur. Assoc. Pet. Geol. 4, 199–208.

Delouis, B., Haessler, H., Cisternas, A., Rivera, L., 1993. Stress tensor determination in France and neighbouring regions. Tectonophysics 221, 413–437.

De Miguel, F., Alguacil, G., Vidal, F., 1988. Una escala de magnitud a partir de la duración para terremotos del sur de España. Rev. Geofis. 44, 75–86.

Díaz, J., Gallart, J., Ruiz, M., Pulgar, J.A., López, C., González-Cortina, J.M., 2002. Anisotropic features of the Alpine lithosphere in northern Spain. Geophys. Res. Lett. 29 (24), 2225, doi:10.1029/2002GL015997.

Díaz, J., Gallart, J., Pedreira, D., Pulgar, J.A., Ruiz, M., López, C., González-Cortina, J.M., 2003. Teleseismic imaging of alpine crustal underthrusting beneath N Iberia. Geophys. Res. Lett. 30 (11), 1554, doi:10.1029/2003GL017073.

ECORS Pyrenees Team, 1988. The ECORS deep reflection seismic survey across the Pyrenees. Nature 331, 508–511.

Engeser, T., Schwentke, W., 1986. Towards a new concept of the tectogenesis of the Pyrenees. Tectonophysics 129, 233–242.

Faci, E., Castiella, J., Del Valle, J., García, A., Díaz, A., Salvany, J.M., Cabra, P., Ramírez del Pozo, J., Meléndez, A., 1997. Mapa geológico de Navarra 1:200.000. Gobierno de Navarra. 142 pp.

Gagnepain, J., Mediano, T., Cisternas, A., Ruegg, J.C., Vadell, M., Hatzfeld, D., Mezcua, J., 1980. Sismicité de la région d'Arette (Pyrénées-Atlantiques) et mécanismes au foyer. Ann. Geofis. 36, 499–508.

Gagnepain-Beyneix, J., Haessler, H., Modiano, T., 1982. The Pyrenean earthquake of February 29, 1980: an example of complex faulting. Tectonophysics 85, 273–290.

Gallart, J., Banda, E., Daignières, M., 1981. Crustal structure of the Paleozoic axial zone of the Pyrenees and transition to the north Pyrenean zone. Ann. Geophys. 37 (3), 457–480.

Gallart, J., Daignières, M., Gagnepain-Beyneix, J., Hirn, A., 1985a. Relationship between deep structure and seismicity in the western Pyrenees. Ann. Geophys. 3 (2), 239–248.

Gallart, J., Diagnières, M., Gagnepain-Beyneix, J., Hirn, A., Olivera, C., 1985b. Seismostructural studies in the Pyrenees: evolution and recent results. PAGEOPH 122 (1984/85), 713–724.

García-Modéjar, J., 1996. Plate reconstruction of the Bay of Biscay. Geology 24, 635–638.

Goldstein, P., Minner, L., 1996. SAC2000: seismic signal processing and analysis tools for the 21st Century. Seismol. Res. Lett. 67, 39.

Goldstein, P., Dodge, D., Firpo, M., Minner, L., 2003. SAC2000: signal processing and analysis tools for seismologists and engineers. In: Lee, W.H.K., Kanamori, H., Jennings, P.C., Kisslinger, C.Invited contribution to "The IASPEI International Handbook of Earthquake and Engineering Seismology", vol. 81B. Academic Press, London.

Gómez, M., Vergés, J., Riaza, C., 2002. Inversion tectonics of the northern margin of the Basque Cantabrian basin. Bull. Soc. Gèol. Fr. t. 173 (5), 449–459.

Grandjean, J., Daignières, M., Gallart, J., Hirn, A., 1994. Répartition de la sismicité dans la partie occidentale des Pyrénées. C. R. Acad. Sci. Paris Ser. II (319), 527–533.

Herraiz, M., Lindo-Ñaupari, G., Giner, R., Simón, J., González-Casado, J.l., Vadillo, J.M., Rodríguez-Pascua, O., Cicuéndez, M.A., Casas, J.I., Cabañas, A., Rincón, L., Cortés, P., Ramírez, A.L., Lucini, M., 2000. The recent (Upper Miocene to Quaternary) and present tectonic stress distributions in the Iberian Peninsula. Tectonics 19, 762–786.

Jabaloy, A., Galindo-Zaldívar, J., González-Lodeiro, F., 2002. Palaeostress evolution of the Iberian Peninsula (Late Carboniferous to present-day). Tectonophysics 357, 159–186.

Jurado, M.J., Müller, B., 1997. Contemporary tectonic stress in northeastern Iberia. New results from borehole breakout analysis. Tectonophysics 282, 99–115.

Larrasoaña, J.C., Parés, J.M., Del Valle, J., Millán, H., 2003. Triassic paleomagnetism from the western Pyrenees revisited: implications for the Iberian–Eurasian Mesozoic plate boundary. Tectonophysics 362, 161–182.

Larrasoaña, J.C., Parés, J.M., Millán, H., Del Valle, J., Pueyo, E.L., 2003. Paleomagnetic, structural, and stratigraphic constraints on transverse fault kinematics during basin inversion: the Pamplona

fault (Pyrenees, north Spain). Tectonics 22 (6), 1071, doi:10.1029/2002TC001446.

Lee, W.H., Lahr, J.C., 1975. HYPO71 (revised): a computer program for determining hypocenters, magnitudes and first motion pattern of local earthquakes. U.S. Geol. Surv. Open File report vol. 75–311, p. 116.

Lee, W.H.K., Bennett, R.E., Meagher, K.L., 1972. A method of estimating magnitude of local earthquakes from signal duration. U.S. Geol. Surv. Open File report, pp. 1–28.

Martínez-Solares, J.M., Mezcua, J., 2003. Catálogo sísmico de la península Ibérica (880 ac-1900). Monografía vol. 18. Instituto Geográfico Nacional, p. 254.

Martínez-Torres, L.M., 1989. El Manto de los Mármoles (Pirineo Occidental): geología estructural y evolución geodinámica. PhD thesis, Univ. País Vasco, Spain. 294 pp.

Matte, P., 1991. Accretionary history and crustal evolution of the Variscan belt in the western Europe. Tectonophysics 196, 309–337.

Mathey, B., Foquet, M., Martínez-Torres, L.M., 1999. The Leiza paleo-fault: role and importance in the Upper Cretaceous sedimentation and paleogeography of the Basque Pyrenees (Spain). C. R. Acad. Sci. Paris 328, 393–399.

Mendia, M.S., Gil-Ibarguchi, J.L., 1991. High-grade metamorphic rocks and peridotites associated to the Leiza fault (western Pyrenees). Geol. Rundsh. 80, 93–107.

Muñoz, J.A., 1992. Evolution of a continental collision belt: ECORS–Pyrenees crustal balanced cross-section. In: McClay, K.R. (Ed.), Thrust Tectonics. Chapman and Hall, London, pp. 235–246.

Muñoz, J.A., 2002. Alpine tectonics I: the Alpine system north of the Betic Cordillera: the Pyrenees. In: Gibbons y, W., Moreno, T. (Eds.), The Geology of Spain. Geological Society, London, pp. 370–385.

Müller, J., Rodgers, P., 1977. L'evolution des Pyrénées (domaine central et occidental). Le segment Hercynien, la chaine de fond alpine. Geol. Alp. 53, 141–191.

Müller, B., Zoback, M.L., Fuchs, K., Mastin, L., Gregersen, S., Pavoni, N., Stephansson, O., Ljunggren, C., 1992. Regional patterns of tectonic stress in Europe. J. Geophys. Res. 97 (B8), 11.783–11.803.

Müller, B., Wehrle, V., Zeyen, H., Fuchs, K., 1997. Short-scale variations of tectonic regimes in the western European stress province north of the Alps and Pyrenees. Tectonophysics 275, 199–219.

Nicolas, M., Santoire, J.P., Delpech, P.Y., 1990. Intraplate seismicity: new seismotectonic data in western Europe. Tectonophysics 179, 27–53.

Olivera, C., Gallart, J., 1987. Sismicidad de la región de Navarra (Pirineos Occidentales). Rev. Geofís. 43, 221–234.

Pedreira, D., Pulgar, J.A., Gallart, J., Díaz, J., 2003. Seismic evidence of Alpine crustal thickening and wedging from the western Pyrenees to the Cantabrian Mountains (north Iberia). J. Geophys. Res. 108 (B4), 2204, doi:10.1029/2001JB001667.

Pedreira, D., 2004. Estructura cortical de la zona de transición entre los Pirineos y la Cordillera Cantábrica. Unpublished PhD Thesis, Univ. Oviedo. Spain. 343 pp.

Pedreira, D., Pulgar, J.A., Gallart, J., Torné, M. Three-dimensional crustal structure of the Western Pyrenees–Cantabrian Mountains probed by gravity/magnetic modelling and seismic constraints. Submitted for publication to Earth Planet. Sci. Lett.

Pous, J., Ledo, J., Marcuello, A., Daignières, M., 1995. Electrical resistivity model of the crust and the upper mantle from a magnetotelluric survey through the central Pyrenees. Geophys. J. Int. 121, 750–762.

Pulgar, J.A., Gallart, J., Fernández-Viejo, G., Pérez-Estaún, A., Álvarez-Marrón, J., 1996. Seismic image of the Cantabrian Mountains in the western extension of the Pyrenees from integrated ESCIN reflection and refraction data. Tectonophysics 264, 1–19.

Rat, P., 1988. The Basque–Cantabrian basin between the Iberian and European plates; some facts but still many problems. Rev. Soc. Geol. Esp. 1 (3–4), 327–348.

Reasenberg, P.A., Oppenheimer, D., 1985. FPFIT, FPPLOT and FPPAGE: Fortran computer programs for calculating and displaying fault-plane solutions. U.S. Geol. Surv. Open File report, vol. 85–739, pp. 25.

Rigo, A., Souriau, A., Dubos, N., Sylvander, M., Ponsolles, C., 2005. Analysis of the seismicity in the central part of the Pyrenees (France), and tectonic implications. J. Seismol. 9, 211–222.

Ruiz, M., Gallart, J., Díaz, J., Pulgar, J.A., González-Cortina, J.M and López, C., submitted for publication. Seismotectonic constraints at the Western edge of the Pyrenees: Aftershock series monitoring of the February 21, 2002 4.1 Lg Earthquake. Geophys. J. Int.

Samardjieva, E., Payo, G., Badal, J., 1999. Magnitude formulae and intensity–magnitude relations for early instrumental earthquakes in the Iberian region. Nat. Hazards 19, 189–204.

Schott, J.J., Peres, A., 1988. Paleomagnetism of Permo-Triassic red beds in the western Pyrenees: evidence for strong clockwise rotations of the Paleozoic units. Tectonophysics 156, 75–88.

Souriau, A., Granet, M., 1995. A tomographic study of the lithosphere beneath the Pyrenees from local and teleseismic data. J. Geophys. Res. 100 (B9), 18.117–18.134.

Souriau, A., Pauchet, H., 1998. A new synthesis of Pyrenean seismicity and its tectonic implications. Tectonophysics 290, 221–244.

Souriau, A., Sylvander, M., Rigo, A., Fels, J.F., Douchain, J.M., Ponsolles, C., 2001. Sismotectonique des Pyrénées: principales constraintes sismologiques. Bull. Soc. Géol. Fr. 172 (1), 25–39.

Srivastava, S.P., Schouten, H., Poest, W.R., Klitgord, K.D., Kovacs, L.C., Verhoef, J., Macnab, R., 1990. Iberian plate kinematics: a jumping boundary between Eurasia and Africa. Nature 344, 756–759.

Street, R., Bollinger, G.A., Woolery, E., 2002. Blasting and other mining-related activities in Kentucky: a source of earthquake misidentification. Seismol. Res. Lett. 73 (5), 739–750.

Teixell, A., 1998. Crustal structure and orogenic material budget in the west central Pyrenees. Tectonics 17 (3), 395–406.

Turner, J.P., 1996. Switches in subduction direction and the lateral termination of mountain belts: Pyrenees–Cantabrian transition, Spain. J. Geol. Soc. 153, 563–571.

Van der Voo, R., Boessenkool, A., 1973. Permian paleomagnetic result from the western Pyrenees delineating the plate boundary between the Iberian peninsula and stable Europe. J. Geophys. Res. 78 (23), 5118–5127.

Vannucci, G., Pondrelli, S., Argnani, A., Morelli, A., Gasperini, P., Boschi, E., 2004. An atlas of the Mediterranean seismicity. Ann. Geophys. 47 (1) (supplement to).

Vergés, J., 2003. Evolución de los sistemas de rampas oblicuas de los Pirineos meridionales: fallas del Segre y Pamplona. Bol. Geol. Min. 114 (1), 87–101.

Waldhauser, F., 2001. HypoDD—a program to compute double-difference hypocenter locations. U.S. Geological Survey. Open File Report, pp. 01–113.

Waldhauser, F., Ellsworth, W.L., 2000. A double-difference earthquake location algorithm: method and application to the northern Hayward fault,California. Bull. Seismol. Soc. Am. 90 (6), 1353–1368.